

# Work Function Dependent Reduction of Transition Metal Nitrides (TMNs) in Hydrogen Environments

Abdul Rehman, Robbert W.E. van de Kruijs, Wesley T.E. van den Beld, Jacobus M. Sturm, and Marcelo Ackermann\*  
*Industrial Focus Group XUV Optics, MESA+ Institute for Nanotechnology,  
University of Twente, Drienerlolaan 5, 7522NB Enschede, the Netherlands*  
(Dated: March 19, 2024)

Amidst the growing importance of hydrogen in a sustainable future, it is critical to develop coatings that can protect system components in reactive hydrogen environments. However, the prediction of the chemical stability of materials in hydrogen is not fully understood. In this study, we show that the work function is a key parameter determining the reducibility (i.e., de-nitridation) of transition metal nitrides (TMNs) in hydrogen radicals ( $H^*$ ). We demonstrate that when the work function of a TMN drops below a threshold limit ( $\phi_{TH}$ ), its reduction effectively stops. This finding provides a novel perspective for comprehending the hydrogen and transition metal compounds interaction and allows predicting the chemical stability of hydrogen-protective coatings.

*Introduction.*-Hydrogen is heralded to play a key role in the green energy transition as either a fuel (fusion) or energy carrier (green hydrogen). Understanding and predicting how hydrogen interacts with materials such as transition metal nitrides (TMNs), which are candidates for hydrogen-protective coatings [1–3] is, therefore, key to fully utilizing hydrogen’s potential for a sustainable future.

The work function is a fundamental parameter of a material system, representing the amount of energy required to transfer an electron from the Fermi level to the vacuum level. Literature indicates a strong correlation between a material’s work function and how hydrogen interacts with it. For instance, based on simulations, Van de Walle et al. showed that the electronic nature of adsorbed hydrogen, forming proton ( $H^+$ ) or hydride ion ( $H^-$ ), is directly dependent on the work function of the surface material for semiconductors and insulators [4, 5]. Furthermore, Kura et al. and Saito et al. experimentally demonstrated that hydrogen in  $TiN_x$ ,  $HfN_x$ , and  $Zr_3N_{4-\delta}$  adsorb as  $H^-$  - forming bonds with transition metal (TM) atoms, proposing that this behavior is due to the materials’ low work functions [6–8].

*Hypothesis.*-In a recent publication [9], we investigated the reduction (de-nitridation) of TMNs in a hydrogen radicals ( $H^*$ ) environment, and proposed that this depends on whether  $H^*$  bind to the TM- or N-atoms (hydrogenation). By expanding the model proposed by Van de Walle et al. [4, 5] to TMN systems, we hypothesize that also for TMNs the hydrogenation pathway is determined by the work function of the host TMN system. This implies that, when the work function of a TMN system is lower than a certain threshold value ( $\phi_{TH}$ ),  $H^*$  favorably form bonds with TM-atoms. This prevents the occurrence of the TMN reduction reaction. However, when the work function of a TMN exceeds  $\phi_{TH}$ , the H-N bond is preferred. If a surface N-atom adsorbs a sufficient ( $x$ ) number of H-atoms, de-nitridation of the TMN

may occur by the formation of  $NH_x$ .

The thermodynamic feasibility of forming  $NH_x$  species then governs the de-nitridation of the TMN, which can be calculated based on the change in the Gibbs free energy ( $\Delta G$ ) for the TMN de-nitridation reaction ( $TMN+xH \rightarrow TM+NH_x$ ). Due to the formation of volatile  $NH_x$  species, N-vacancies form at the surface. The subsurface N-atoms then diffuse to the surface, filling the vacancies and leading to further de-nitridation. However, as (electronegative) N-atoms are removed from the TMN system, its work function progressively decreases, potentially reaching  $\phi_{TH}$ . Consequently, the reduction reaction is self-limiting and ultimately stops.

In the present study, we experimentally show that the reduction of TMNs leads to a drop in work function, and that the de-nitridation reaction effectively stops when their work function reaches  $4.3\pm 0.4$  eV ( $\phi_{TH}$ ). We exposed  $5\pm 0.5$  nm thin films of TiN, TaN, and NbN with  $\approx 2$  nm surface oxynitride layers to  $H^*$  at 700 °C and 0.02 mbar of working pressure. Under these experimental conditions, TiN is non-reducible due to its low work function ( $< \phi_{TH}$ ), while the de-nitridation of TaN and NbN readily occurred. Nonetheless, for TaN and NbN, the de-nitridation stops once their work functions drop to  $\phi_{TH}$ .

*Methodology.*- TiN, TaN, and NbN thin films are deposited via reactive DC magnetron sputtering onto Si(100) substrates. The base pressure of the deposition chamber is in the low  $10^{-8}$  mbar range for all the depositions. Ar (99.999 %) and  $N_2$  (99.999 %) with a flow rate of 15 sccm are used as sputtering gases. The working pressure during the depositions is  $10^{-3}$  mbar.  $5\pm 0.5$  nm TMN thin films are deposited, where the thickness is controlled by deposition time and the deposition rates were in advance calibrated via X-ray reflectivity measurements. The measurements are performed using a Malvern Panalytical Empyrean laboratory diffractometer, which uses monochromatic Cu-K $\alpha$ 1 radiation. The thickness of the films is chosen such that the full depth of the films is probed by angle-resolved X-ray photoelec-

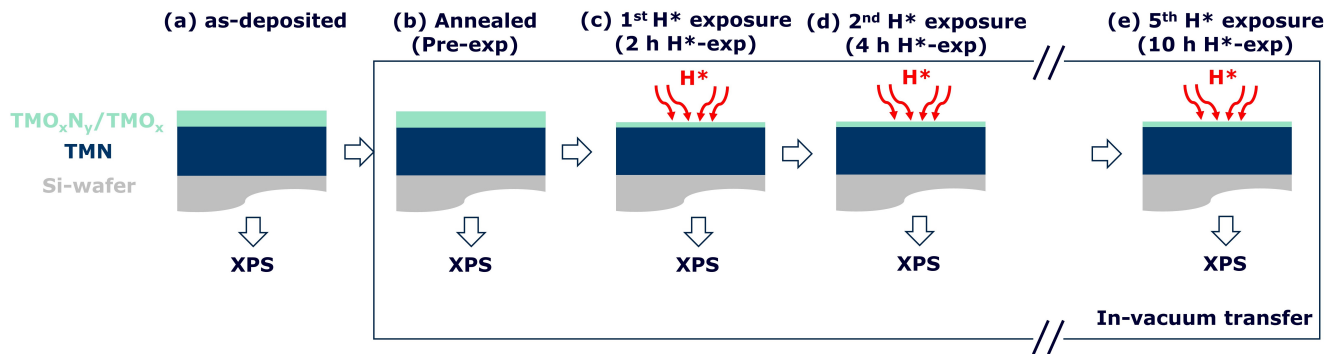


FIG. 1. Schematic of methodology. (a) TMN samples are deposited via reactive DC magnetron sputtering. Thin  $\text{TMO}_x\text{N}_y/\text{TMO}_x$  layers form on the samples' surfaces during ambient transfer. (b) TMN samples are annealed at  $700^\circ\text{C}$ . (c-e) Samples are repeatedly exposed to  $\text{H}^*$  at  $700^\circ\text{C}$  for 2 h until no further change in their stoichiometry is observed. AR-XPS measurements are performed on the samples after each process (annealing/ $\text{H}^*$ -exposure).

tron spectroscopy (AR-XPS), which uses a monochromatic  $\text{Al-K}\alpha$  radiation source with a spot size of  $400\ \mu\text{m}$ . AR-XPS measurements are performed using ThermoFisher Theta probe angle-resolved X-ray photoelectron spectrometer. After depositions, the samples are transferred through air to the load-lock of the exposure and XPS vacuum chambers. The exposure to ambient is minimized ( $< 0.5\ \text{h}$ ) to limit surface oxidation (Fig. 1a).

From the load-lock, the samples are transported to the exposure chamber via a vacuum of low  $10^{-9}$  mbar. In the exposure chamber, the samples are then first annealed at  $700^\circ\text{C}$ . The purpose of annealing is to saturate all thermally induced processes before high-temperature  $\text{H}^*$ -exposures. The base pressure of the exposure chamber is in the low  $10^{-8}$  mbar range. The samples are annealed at  $700^\circ\text{C}$  for 2 h with a base pressure of low  $10^{-7}$  mbar during annealing. The sample temperature is measured via a N-type thermocouple which is clamped on the sample surface. After annealing, the samples cool down to approximately  $100^\circ\text{C}$  and are then transferred to the AR-XPS chamber (low  $10^{-9}$  mbar). The corresponding AR-XPS measurements are referred to as 'pre-exposed' (or pre-exp) in the text and figures (Fig. 1b).

The pre-exposed samples are transferred back to the exposure chamber in-vacuo for  $\text{H}^*$ -exposure.  $\text{H}^*$  in the chamber are generated by thermally cracking  $\text{H}_2$  with a W-filament heated to  $\approx 2000^\circ\text{C}$ . The samples are placed  $\approx 5\ \text{cm}$  from the cracking filament. The working pressure was set at 0.02 mbar, corresponding to a  $\text{H}^*$  flux impinging on the sample surface of  $10^{21\pm 1}\ \text{H}^*\ \text{m}^{-2}\text{s}^{-1}$  [9]. The samples are exposed to  $\text{H}^*$  at  $700^\circ\text{C}$  for 2 h. The  $\text{H}^*$ -exposure conditions are set so that the results are relevant to fusion reactors and EUV scanners [1, 10–12]. After the  $\text{H}^*$ -exposure, samples cool down to about  $100^\circ\text{C}$  and are transferred to the AR-XPS chamber via vacuum. The corresponding AR-XPS measurements are referred to as '2 h  $\text{H}^*$ -exposed' (2 h  $\text{H}^*$ -exp) in the text and figures (Fig. 1c).

To assess further de-nitridation as a function of  $\text{H}^*$ -exposure, the samples are repeatedly exposed to  $\text{H}^*$  in a similar manner ( $700^\circ\text{C}$  for 2 h) until no significant change in the chemical composition of the samples is observed (Figs. 1d and 1e). AR-XPS measurements are performed on the samples after each exposure, which are labelled after the total  $\text{H}^*$ -exposure time.

Changes in the stoichiometry of the samples are evaluated based on the core-level TM, N1s, and O1s AR-XPS spectra. Core-level TM and N1s XPS spectra taken at a take-off angle ( $\Theta$  from the surface normal) of  $34.25^\circ$  are discussed in detail in the text. The corresponding fitted peak positions are provided in the supplementary information (Table. SI1-3). A comparison between core level TM, N1s, O1s, and Si2p XPS spectra taken over the range of AR-XPS measurements ( $\Theta$  ranging from  $26.75^\circ$  to  $71.75^\circ$ , providing probing depth from  $\approx 5$  to  $\approx 1.5\ \text{nm}$ , respectively) before and after  $\text{H}^*$ -exposures is also provided in the supplementary information (Fig. SI 5-7). To quantify N- and O-atomic losses, the ratios between at.% of N and TM (N/TM) and at.% of O and TM (O/TM) are calculated over the range of AR-XPS measurements. Changes in the N/TM ratios are discussed in the text, while O/TM ratios are provided in the supplementary information (Fig. SI 2-4). The at.% of N in the samples is measured by considering the area under the TMN/ $\text{TMO}_x\text{N}_y$  peak in the N1s spectra of the samples and the corresponding sensitivity factor. The whole area under the O1s spectra is used for determining the amount of O-atoms in the samples. Nb at.% in the NbN samples is also calculated by taking the whole area under the Nb3d spectra. Due to the presence of the satellite feature (TiN-sat) in the Ti2p spectra and the O2s peak in the Ta4f spectra, the cumulative areas under the main peaks of TMN-,  $\text{TMO}_x\text{N}_y/\text{TMO}_{x-\delta}$ -, and  $\text{TMO}_x$ - doublets along with their sensitivity factors are used for calculating the at.% of Ti and Ta in the samples.

The work function of the samples is measured via XPS

[13]. A negative bias of 16.4 V is applied while collecting valence band (VB) and low kinetic energy (LKE) spectra. To account for this bias, VB spectra are also collected without any applied bias. Since TMN samples are sufficiently conductive, the Fermi level of the unbiased samples is set as the reference point at zero binding energy. To ensure consistency, the binding energy of the biased sample is adjusted to align with the Fermi level of the unbiased sample (LKE and VB spectra of the samples are provided in the supplementary information (Fig. SI 8)). In our instrument, the sample plane is not parallel to the entrance of the electron analyzer, which leads to a systematic deviation between the measured and actual work function according to ref. [13, 14]. By comparing the measured and reported work functions of sputter-cleaned polycrystalline foils of Au, Cu, and Ag (Table. SI 4, Fig. SI 9-10), we determined this systematic offset in the measured work function to be  $-1.0 \pm 0.2$  eV. The work function values presented in the text and figures have already been adjusted to account for this offset and the 0.1 eV uncertainty associated with the measured secondary electron cutoff.

*Results and discussions.*- De-oxidation of surface oxynitrides is predominantly observed in the TiN sample after 2 h  $H^*$ -exposure, which results in an increase in the TiN fraction in the XPS probing depth (Fig. 2a and SI2). Due to the removal of O-atoms from the system, the work function drops to  $4.2 \pm 0.3$  eV (Fig. 2b). Notably, no further change in the chemical composition of the sample is observed afterward. TaN and NbN samples undergo de-nitridation, besides de-oxidation (Fig. 2a, SI3, and SI4). However, de-nitridation of the TaN and NbN samples effectively stops as their work functions drop to  $4.3 \pm 0.3$  eV and  $4.4 \pm 0.3$  eV, respectively (Fig. 2). In the subsequent paragraphs, we discuss each sample in detail.

Fig. 3 shows the Ti2p and N1s XPS spectra of the TiN sample at  $\Theta=34.25^\circ$ , along with the N/Ti ratio calculated over the range of AR-XPS measurement and the measured work functions of the pre- and post- $H^*$ -exposed TiN sample. The work function of the pre-exposed (0 h) TiN sample is  $4.9 \pm 0.3$  eV (Fig. 3d), which is in line with the reported work function of ambient-exposed TiN (with surface oxides/oxynitrides) [15]. According to our hypothesis,  $H^*$  adsorb on surface O- and N-atoms due to the high work function of the sample. As the formation of O-vacancies is energetically more favorable than N-vacancies on this  $TiO_xN_y$  layer (Fig. SI 1), the pre-exposed TiN sample first shows de-oxidation upon 2 h  $H^*$ -exposure (Fig. 3a and SI 2). De-oxidation of the surface results in an increase in the TiN fraction over the XPS probing depth, which is apparent from an increase in the intensity of the TiN doublet in Ti2p and the N/Ti ratio after 2 h of  $H^*$ -exposure (Fig. 3a and 3c). A slight shift in the TiN/TiON peak towards higher binding energy is also due to the drop in the O-fraction (Fig. 3a, 3b, and SI2). Because of the surface de-oxidation followed by

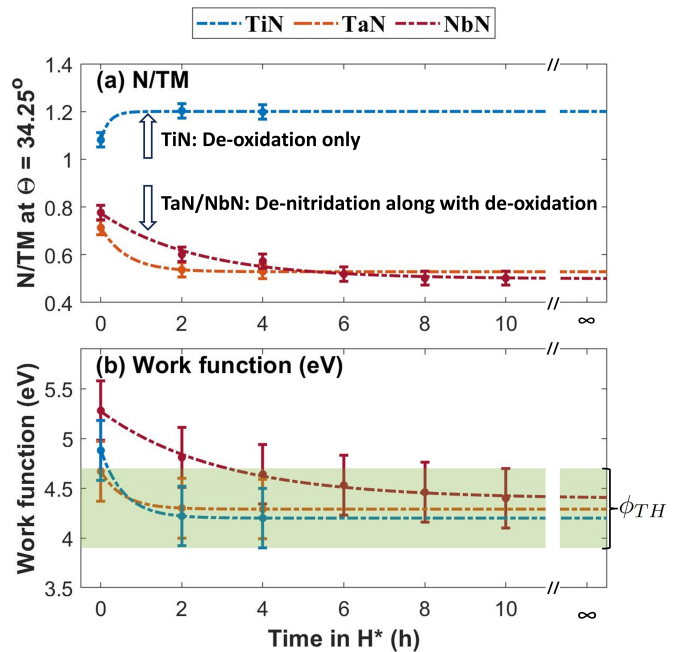


FIG. 2. (a) N/TM ratio in the samples measured at  $\Theta=34.25^\circ$ , before and after  $H^*$ -exposures, and (b) the corresponding measured work functions of the TiN (in blue), TaN (in orange), and NbN (in maroon) samples. The N/Ti ratio increases after 2 h of  $H^*$ -exposure due to de-oxidation of the surface oxynitrides. The work function of the 2 h  $H^*$ -exposure sample is  $4.2 \pm 0.3$  eV, and no further change in the stoichiometry of the sample is noted. In contrast, besides de-oxidation, de-nitridation of the TaN and NbN samples occurs until their work functions drop to  $4.3 \pm 0.3$  eV and  $4.4 \pm 0.3$  eV, respectively. The fitted exponential curves show that the TMN reduction reaction effectively stops as the work function approaches  $\phi_{TH}$

the diffusion of subsurface N-atoms to the surface vacancies, the surface stoichiometry of the sample changes from approximately  $TiO_{0.95}N_{0.86}$  to  $TiO_{0.76}N_{1.1}$  (measured at  $\Theta = 71.75^\circ$ ). The removal of O-atoms (more electronegative than N-atoms) leads to a drop in the work function of the sample by  $0.7 \pm 0.2$  eV (Fig. 3d and SI8). The work function of the sample after 2 h  $H^*$ -exposure is  $4.2 \pm 0.3$  eV (Fig. 3d), which is close to the work function reported for pristine TiN [6]. After 2 h of  $H^*$ -exposure, the reduction reaction effectively stops, as evident from the stabilization of the stoichiometry of the sample. Consistent with our hypothesis, this is due to the preferred  $H^*$  binding to TM-atoms since the work function of the sample after 2 h of  $H^*$ -exposure is already low.

In contrast to the TiN sample which predominantly shows de-oxidation, the TaN, and the NbN samples did show de-nitridation. The work functions of the pre-exposed TaN and NbN samples are  $4.7 \pm 0.3$  eV and  $5.3 \pm 0.3$  eV, respectively (Fig. 4d, 5d). These values

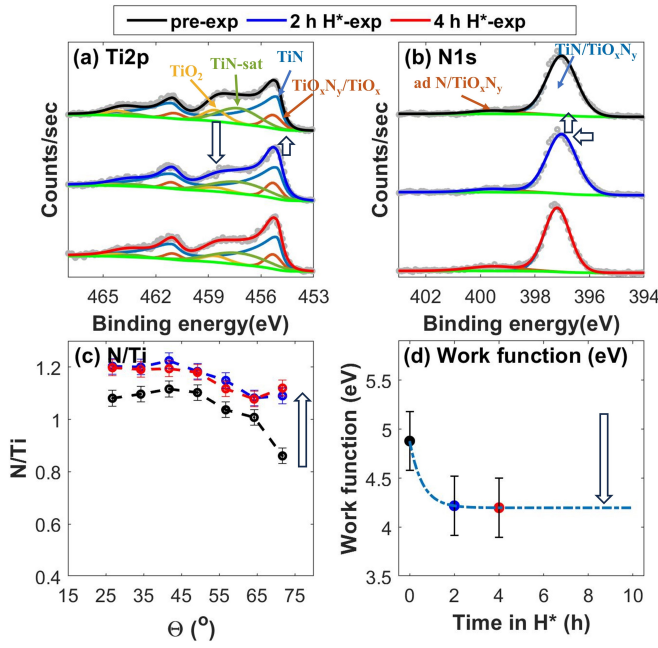


FIG. 3. (a-b) XPS spectra of pre-exposed (black), 2 h H\*-exposed (in blue), and 4 h H\*-exposed (in red) TiN sample taken at  $\Theta=34.25^\circ$  along with (c) variation in N/Ti ratio over the range of AR-XPS measurements and (d) measured work functions before and after H\*-exposures. Reduction of surface oxides during 2 h H\*-exposure results in an increase in TiN content in the XPS probing depth and a decrease in the work function to  $4.2\pm 0.3$  eV. No significant change in the XPS spectra and N/Ti after 2 h H\*-exposure indicates that TiN<sub>1.2</sub> (measured at  $\Theta = 34.25^\circ$ ) is non-reducible under the performed experimental conditions. The non-reducibility of TiN is attributed to its low work function.

are in close agreement with the reported work functions of ambient exposed TaN and NbN thin films with surface oxides/oxy-nitrides [15]. As per our hypothesis, H\* preferably adsorb on surface O- and N-atoms, attributed to the high work functions of the samples. The formation of H<sub>2</sub>O is energetically favorable over NH<sub>3</sub> on O-rich Ta- and Nb- oxynitride surfaces (Fig. SI 1) [9], which results in the de-oxidation of the surface oxynitrides. The de-oxidation of the samples is evident from the decrease in the intensity of Ta<sub>2</sub>O<sub>5</sub> and Nb<sub>2</sub>O<sub>5</sub> doublets and O/TM ratios after 2 h H\*-exposure (Fig. 4a, 5a, SI3, and SI4). Since the work functions of pristine TaN and NbN are high ( $> 4.5$  eV) [16], in alignment with our hypothesis, de-nitridation of the samples occurs after de-oxidation. The shift in the TaN<sub>x</sub> and NbN<sub>x</sub> doublets towards 0.5 eV and 0.2 eV lower binding energies, respectively, and a drop in the N/TM ratio indicate de-nitridation (Fig. 4a, 4c, 5a, and 5c) of the samples. Furthermore, owing to the de-oxidation of surface oxynitrides, TaN/TaON and

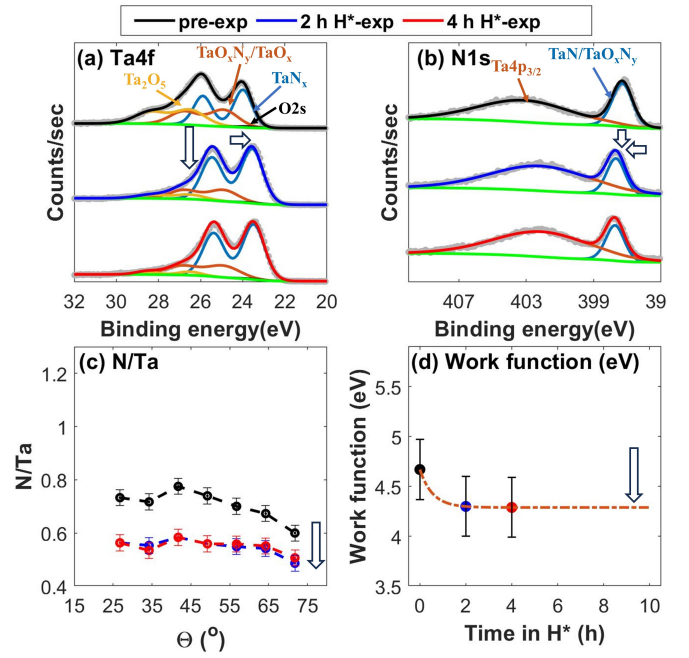


FIG. 4. (a-b) XPS spectra of pre-exposed (in black), 2 h H\*-exposed (in blue), and 4 h H\*-exposed (in red) TaN sample taken at  $\Theta=34.25^\circ$  along with (c) variation in N/Ta ratio over the range of AR-XPS measurements and (d) measured work functions before and after H\*-exposures. Surface de-oxidation along with subsurface denitridation is observed upon 2 h H\*-exposure. Following 2 h H\*-exposure, the work function of the sample is measured to be  $4.3\pm 0.3$  eV. Because of the low work function, the sample is not reduced any further.

NbN/NbON peaks in the N1s spectra are also shifted by 0.4 eV higher binding energy (Fig. 4b and 5b). Due to the reduction of the surface, the surface stoichiometry of the samples shifts from approximately TaO<sub>0.87</sub>N<sub>0.60</sub> and NbO<sub>0.47</sub>N<sub>0.75</sub> to TaO<sub>0.42</sub>N<sub>0.49</sub> and NbO<sub>0.23</sub>N<sub>0.62</sub> (measured at  $\Theta = 71.75^\circ$ ). Additionally, the work functions of the TaN and NbN samples drop by  $0.4\pm 0.2$  eV and  $0.5\pm 0.2$  eV, respectively upon 2 h H\*-exposure (Fig. 4d, 5d, and SI8).

The work function of the TaN sample after 2 h H\*-exposure is  $4.3\pm 0.3$  eV (Fig. 4d), and no further reduction of the sample is observed (Fig. 4). However, the NbN sample continues de-nitridation over 8 h H\*-exposure until its work function reaches  $4.4\pm 0.3$  eV (Fig. 5). Hence, de-nitridation of the TaN and the NbN samples effectively stops when their work functions drop to  $4.3\pm 0.3$  eV and  $4.4\pm 0.3$  eV, respectively.

*Conclusion.-* We show that the reduction of a TMN system in H\* effectively stops when its work function drops to  $4.3\pm 0.4$  eV. The value strikingly aligns with the reported  $4.4\pm 0.2$  eV work function, where H<sup>+</sup> and H<sup>-</sup> in semiconductors and insulators have equal formation

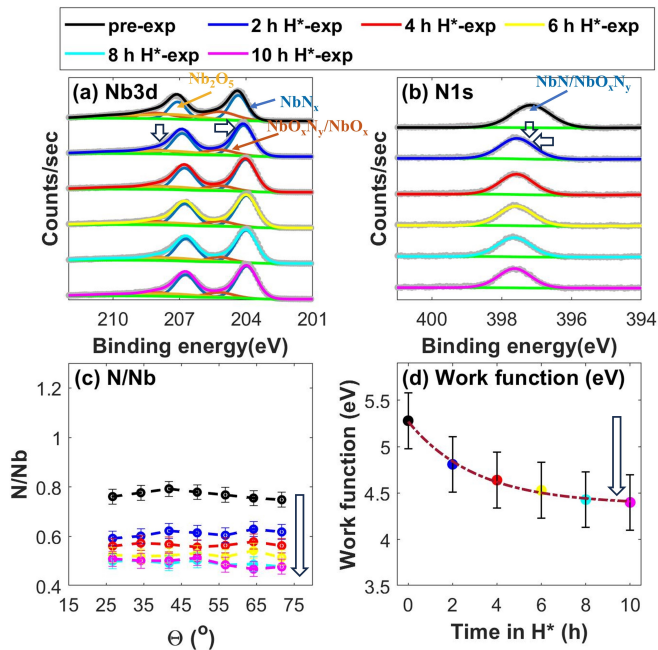


FIG. 5. (a-b) XPS spectra of pre-exposed (in black), 2 h H<sup>\*</sup>-exposed (in blue), 4 h H<sup>\*</sup>-exposed (in red), 6 h H<sup>\*</sup>-exposed (in yellow), 8 h H<sup>\*</sup>-exposed (in cyan), and 10 h H<sup>\*</sup>-exposed (in magenta) NbN sample taken at a  $\Theta=34.25^\circ$  along with (c) variation in N/Nb ratio over the range of AR-XPS measurements and (d) measured work functions before and after H<sup>\*</sup>-exposures. De-nitridation of the sample is observed until its work function drops to  $4.4\pm 0.3$  eV.

energies, as proposed in [4, 5]. Thus, we propose that the reduction reactions of TMNs depend on whether H<sup>\*</sup> form bonds with TM- or N-atoms (hydrogenation), determined by the work function of the host material. Furthermore, we propose that when the work function drops to a threshold ( $\phi_{TH}$ ), due to chemical alteration of the surface, H<sup>\*</sup> preferably bind to TM-atoms, rather than N-atoms. This effectively stops the reduction reaction of the TMNs, showing a stable TMNs surface stoichiometry, as no volatile species form from binding H<sup>\*</sup> to the TM-atoms. We hypothesize that this model holds for a wider range of transition metal compounds (TMX, where X = O or C), using the work function as a key parameter for predicting materials' stability for hydrogen-protective coatings.

*Acknowledgments.*-This work has been carried out in the frame of the Industrial Partnership Program “X-tools,” project no. 741.018.301, funded by the Netherlands Organization for Scientific Research, ASML, Carl Zeiss SMT, and Malvern Panalytical.

\* m.d.ackermann@utwente.nl

- [1] V. Nemanič, Hydrogen permeation barriers: Basic requirements, materials selection, deposition methods, and quality evaluation, *Nuclear Materials and Energy* **19**, 451 (2019).
- [2] T. Zhou, D. Liu, Y. Zhang, T. Ouyang, and J. Suo, Microstructure and hydrogen impermeability of titanium nitride thin films deposited by direct current reactive magnetron sputtering, *Journal of Alloys and Compounds* **688**, 44 (2016).
- [3] J. Matějček, J. Veverka, V. Nemanič, L. Cvrček, F. Lukáč, V. Havranek, and K. Illkova, Characterization of less common nitrides as potential permeation barriers, *Fusion Engineering and Design* **139**, 74 (2019).
- [4] C. G. Van de Walle and J. Neugebauer, Universal alignment of hydrogen levels in semiconductors, insulators and solutions, *Nature* **423**, 626 (2003).
- [5] C. G. Van de Walle, Universal alignment of hydrogen levels in semiconductors and insulators, *Physica B: Condensed Matter* **376**, 1 (2006).
- [6] C. Kura, Y. Kunisada, E. Tsuji, C. Zhu, H. Habazaki, S. Nagata, M. P. Müller, R. A. De Souza, and Y. Aoki, Hydrogen separation by nanocrystalline titanium nitride membranes with high hydride ion conductivity, *Nature Energy* **2**, 786 (2017).
- [7] C. Kura, S. Fujimoto, Y. Kunisada, D. Kowalski, E. Tsuji, C. Zhu, H. Habazaki, and Y. Aoki, Enhanced hydrogen permeability of hafnium nitride nanocrystalline membranes by interfacial hydride conduction, *Journal of Materials Chemistry A* **6**, 2730 (2018).
- [8] M. Saito, C. Kura, H. Toriumi, S. Hinokuma, T. Ina, H. Habazaki, and Y. Aoki, Formation of mobile hydridic defects in zirconium nitride films with n-type semiconductor properties, *ACS Applied Electronic Materials* **3**, 3980 (2021).
- [9] A. Rehman, R. W. van de Kruijs, W. T. van den Beld, J. M. Sturm, and M. Ackermann, Chemical interaction of hydrogen radicals (h<sup>\*</sup>) with transition metal nitrides, *The Journal of Physical Chemistry C* (2023).
- [10] D. Brouns, A. Bendiksen, P. Broman, E. Casimiri, P. Colsters, P. Delmastro, D. de Graaf, P. Janssen, M. van de Kerkhof, R. Kramer, *et al.*, Nxe pellicle: offering a euv pellicle solution to the industry, in *Extreme Ultraviolet (EUV) Lithography VII*, Vol. 9776 (SPIE, 2016) pp. 567–576.
- [11] C. Zoldesi, K. Bal, B. Blum, G. Bock, D. Brouns, F. Dhalluin, N. Dziomkina, J. D. A. Espinoza, J. de Hoogh, and S. Houweling, Progress on euv pellicle development, in *Extreme Ultraviolet (EUV) Lithography V*, Vol. 9048 (SPIE) pp. 430–439.
- [12] M. van de Kerkhof, A. M. Yakunin, V. Kvon, A. Nikipelov, D. Astakhov, P. Krainov, and V. Banine, Euv-induced hydrogen plasma and particle release, *Radiation Effects and Defects in Solids* **177**, 486 (2022).
- [13] J. W. Kim and A. Kim, Absolute work function measurement by using photoelectron spectroscopy, *Current Applied Physics* **31**, 52 (2021).
- [14] M. Helander, M. Greiner, Z. Wang, and Z. Lu, Pitfalls in measuring work function using photoelectron spectroscopy, *Applied Surface Science* **256**, 2602 (2010).
- [15] R. Fujii, Y. Gotoh, M. Liao, H. Tsuji, and J. Ishikawa,

Work function measurement of transition metal nitride and carbide thin films, *Vacuum* **80**, 832 (2006).

- [16] T. Hino, T. Yamashina, S. Fukuda, and Y. Takasugi, Chemical sputtering and radiation enhanced sublimation

of graphite due to hydrogen ions, *Journal of nuclear materials* **186**, 54 (1991).